Supporting Information for

# Effectiveness of Ammonia Reduction on Control of Fine Particle Nitrate

Hongyu Guo[1], Rene Otjes[2], Patrick Schlag[3,4,5], Astrid Kiendler-Scharr[4], Athanasios Nenes[1,6,7,8], Rodney J. Weber[1]

[1] School of Earth and Atmospheric Sciences, Georgia Institute of Technology, Atlanta, GA 30332, USA
[2] Energy Research Centre of the Netherlands (ECN), Petten, Netherlands
[3] Utrecht University, Utrecht, Netherlands
[4] Institute for Energy and Climate Research (IEK-8): Troposphere, Forschungszentrum Jülich, Jülich, Germany
[5] Now at University of Sao Paulo, SP, Brazil
[6] School of Chemical and Biomolecular Engineering, Georgia Institute of Technology, Atlanta, GA 30332, USA
[7] Institute for Chemical Engineering Sciences, Foundation for Research and Technology – Hellas, Patras, GR-26504, Greece
[8] Institute for Environmental Research and Sustainable Development, National Observatory of Athens, P. Penteli, Athens, GR-15236, Greece

* *To whom correspondence should be addressed: [rweber@eas.gatech.edu](mailto:rweber@eas.gatech.edu)*

## Contents of this file

**Figures S1-S8**

**Table S1**

## 1. Diurnal profiles of T, RH and pH in Cabauw, Netherlands
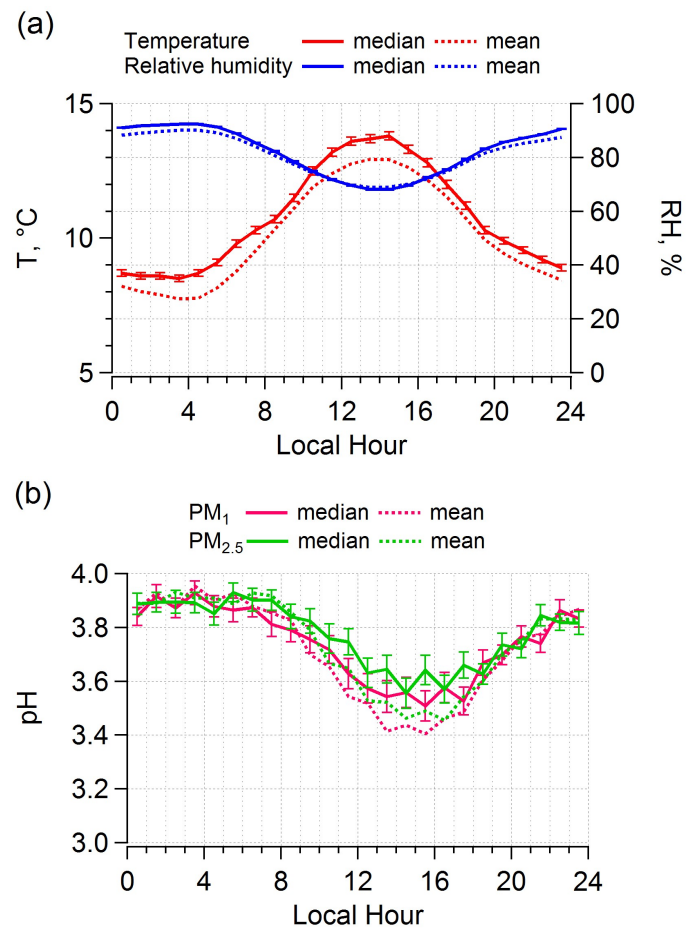
**Fig. S1.** For the one-year observation at CESAR tower, diurnal profiles of (a) measured T, RH, (b) predicted $PM_1$ and $PM_{2.5}$ pH. Mean hourly medians and means are shown and standard errors are plotted as error bars.

## 2. The thermodynamic model and comparison of predicted and measured gas-particle partitioning in Cabauw, Netherlands

pH of $PM_1$ or $PM_{2.5}$ was determined from running the Windows stand-alone executable version of ISORROPIA-II (http://isorropia.eas.gatech.edu/index.php?title=Main_Page) in forward and metastable modes. The model has been proven to accurately predict gas-aerosol partitioning of inorganic species in many studies (Fountoukis and Nenes, 2007; Guo et al., 2016; Guo et al., 2017a; Liu et al., 2017), including particle liquid water (Guo et al., 2015; Bougiatioti et al., 2016). ISORROPIA-II has been used to predict particle pH in several studies (Guo et al., 2015; Hennigan et al., 2015; Guo et al., 2016; Guo et al., 2017a; Liu et al., 2017). pH is a logarithmic scale of hydronium ion activity in an aqueous solution,

$$pH = -\log_{10} \gamma_{H^+} H_{aq}^+ = -\log_{10} \frac{1000 \gamma_{H^+} H_{air}^+}{W_i + W_o} \cong -\log_{10} \frac{1000 \gamma_{H^+} H_{air}^+}{W_i} \qquad (1)$$

where $\gamma_{H^+}$ is the hydronium ion activity coefficient. $\gamma_{H^+}$ is assumed = 1, however, ISORROPIA-II calculates the activity coefficients of ionic pairs, such as $H^+$-$NO_3^-$, so the nonideality effect of $H^+$ is considered), $H_{aq}^+$ (mol $L^{-1}$) is the hydronium ion concentration in particle liquid water, $H_{air}^+$ ($\mu g\ m^{-3}$) is the hydronium ion concentration per volume of air, and $W_i$, $W_o$ ($\mu g\ m^{-3}$) are particle water concentrations associated with inorganic and organic species, respectively. pH predicted solely with $W_i$ is fairly accurate; pH was 0.15-0.23 units systematically lower than and highly correlated to ($r^2 = 0.97$) pH predicted with total particle water ($W_i + W_o$) in the southeastern US, where $W_o$ was on average 35% of total particle water (Guo et al., 2015). In most other location, including this study, a smaller contribution from $W_o$ is expected based on the smaller organic aerosol mass fraction, 29%, (Schlag et al., 2016) compared to the southeastern US, ~60% (Xu et al., 2015). For this study of Cabauw, we only use $W_i$ for the following pH calculations.

As in past studies (Guo et al., 2015; Guo et al., 2016; Guo et al., 2017a), predicted pH was assessed by comparing measured and model-predicted gas-aerosol partitioning of semi-volatile species, such as $NH_3$-$NH_4^+$, $HNO_3$-$NO_3^-$, $HCl$-$Cl^-$, when not completely in the gas or aerosol phase. An accurate pH prediction is important in this study, as the nitrate gas-particle partitioning is pH dependent (Guo et al., 2016).
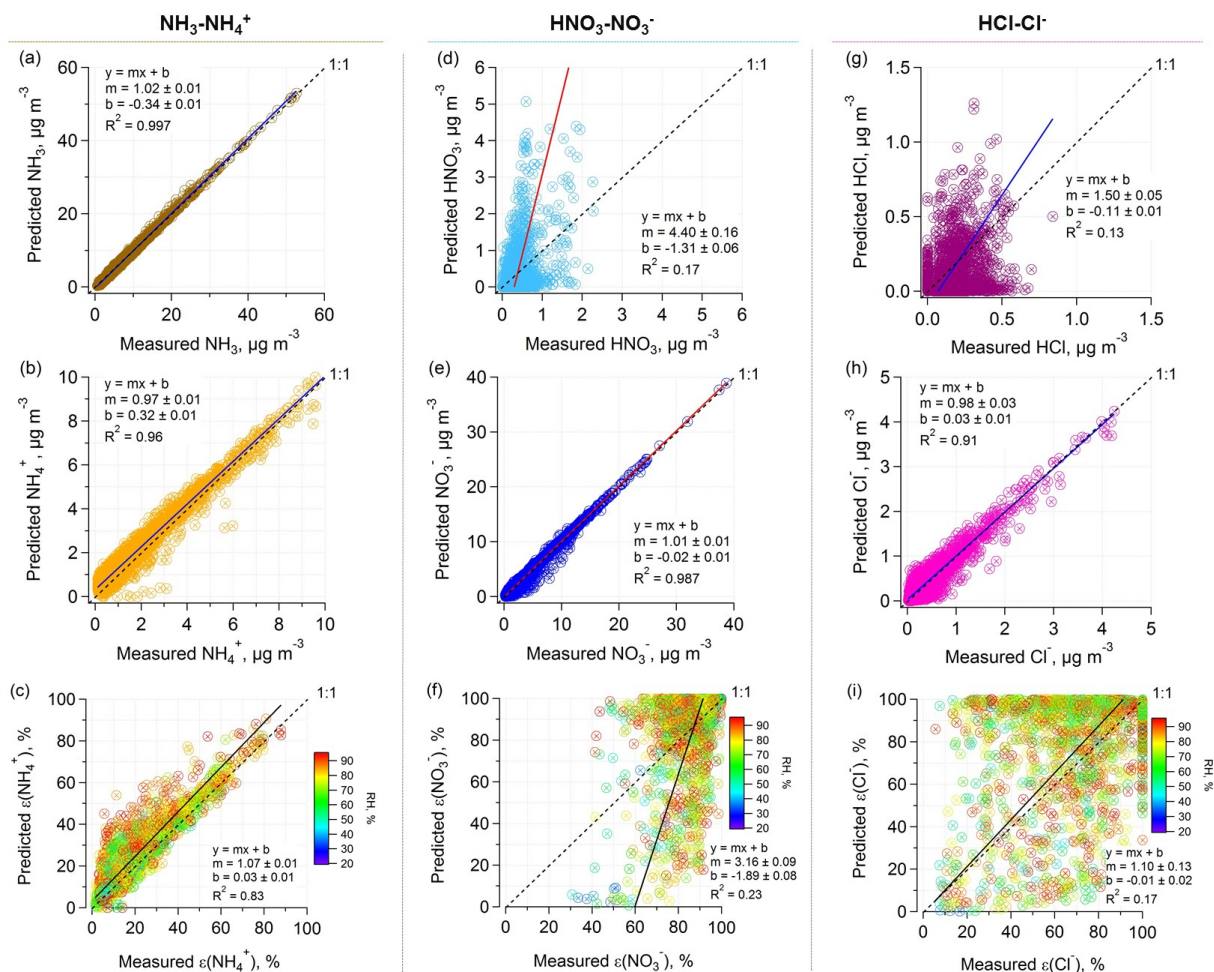
**Fig. S2.** Comparisons of predicted and measured $NH_3$, $NH_4^+$, and $\varepsilon(NH_4^+)$ (a, b, c), $HNO_3$, $NO_3^-$, and $\varepsilon(NO_3^-)$ (d, e, f), and $HCl$, $Cl^-$, and $\varepsilon(Cl^-)$ (g, h, i) for data from the one-year observational study at CESAR ground site. Gas- and particle-phase ($PM_{2.5}$) data are all from MARGA. Low concentrations within 2×LOD are excluded in plotting particle phase fractions due to high uncertainties. Orthogonal distance regression (ODR) fits are shown and uncertainties in the fits are one standard deviation (SD). Less agreement for gas phase $HNO_3$ and $HCl$ are thought to be due to significantly lower concentrations than the particle phase component ($NO_3^-$, $Cl^-$, respectively). Bias in these gases can be possible if some particles are captured in the denuder, given that the ion chromatographic detection system can not distinguish between gas and particle phases ($NO_3^-$ and $Cl^-$ is measured for both).
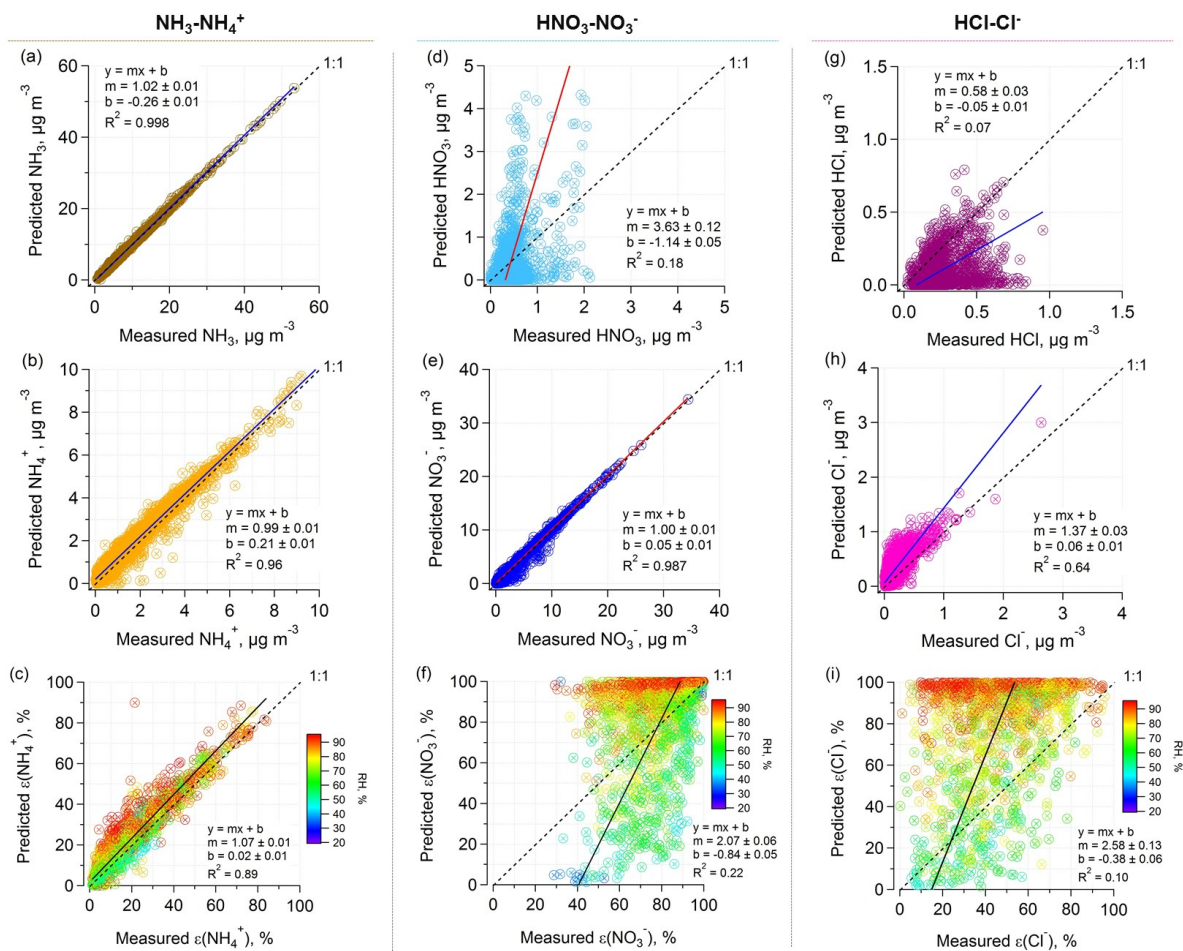
**Fig. S3.** A similar plot as Fig. S2. MARGA PM$_1$ data was used in the model input instead of PM$_{2.5}$.

### 3. Analytically predicted nitrate partitioning versus pH for various field studies
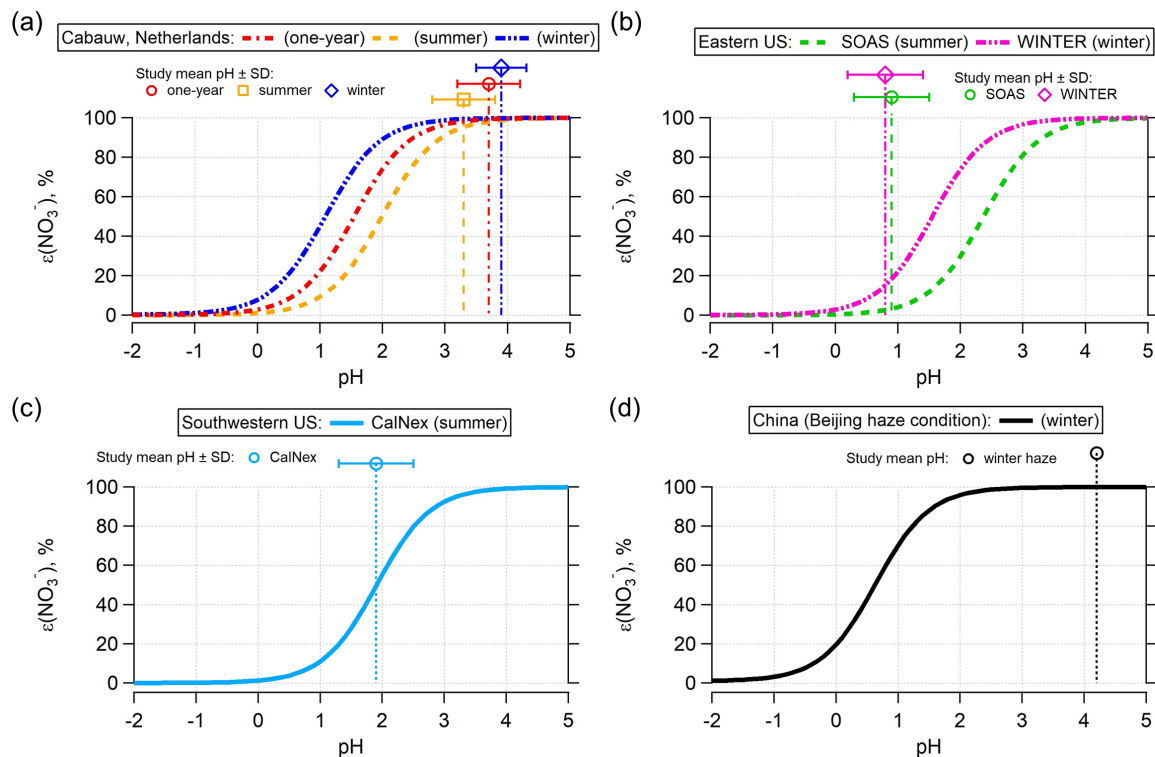
**Fig. S4.** $\varepsilon(NO_3^-)$ versus pH for the listed field studies. The S curves are calculated based on the average temperature, liquid water, and activity coefficients for each study, according to Eq. (4). The input can be found in Table S1. Vertical lines are the study average ambient fine particle pH calculated with ISORROPIA-II and error bars show the variability in pH as one standard deviation. This figure is reproduced from Figure 2 in the main text, to directly show the seasonal variations at a specific region.

## 4. Comparison of ISORROPIA-II predicted and analytically predicted pH
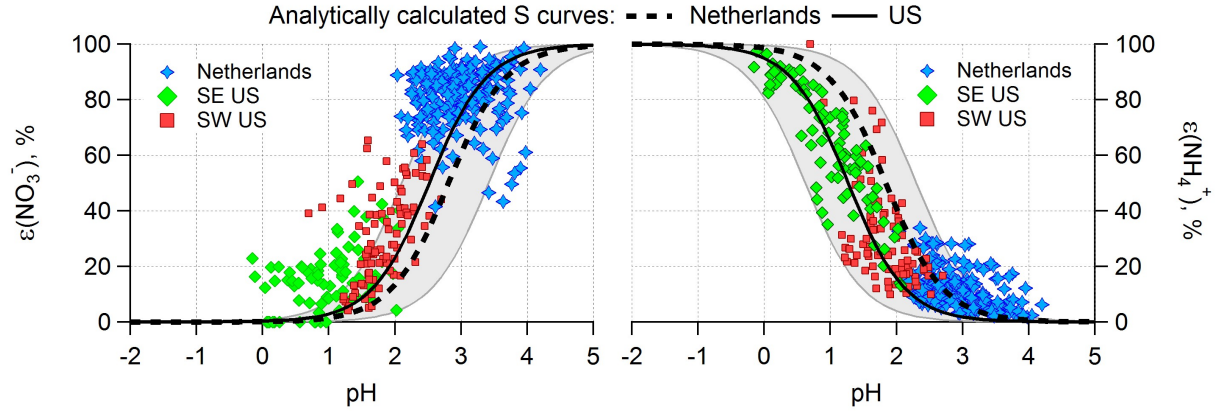
**Fig. S5.** Analytically calculated S curves of $\varepsilon(NO_3^-)$ and $\varepsilon(NH_4^+)$ (shown as lines), and observed ambient $\varepsilon(NO_3^-)$ and $\varepsilon(NH_4^+)$ plotted with ISORROPIA-predicted pH for SOAS (SE US), CalNex (SW US), and this study at Cabauw (Netherlands) (shown as data points). $\varepsilon(NO_3^-)$ and $\varepsilon(NH_4^+)$ are the particle fraction of gas plus particle for nitrate and ammonium, respectively. The analytical calculations are based on simple thermodynamic equations that can be found in the main text, Eq. (4) for $\varepsilon(NO_3^-)$ or in Guo et al. (2017a) and are independent of ISORROPIA-II calculations. Plotted data are for a relatively narrow range in $W_i$ (1 to 4 µg m$^{-3}$) and T (15 to 25 °C) for comparison with the analytical calculation based on $W_i = 2.5$ µg m$^{-3}$ and T = 20 °C. For the analytical calculations (the black solid and dashed S curves), ISORROPIA-II predicted activity coefficients are applied. For the selected water and temperature ranges, $\gamma_{H^+}\gamma_{NO_3^-}$ is $0.17 \pm 0.10$ for Cabauw, $0.086 \pm 0.060$ for SE US, and $0.087 \pm 0.027$ for SW US and $\gamma_{H^+}/\gamma_{NH_4^+}$ is $5.93 \pm 6.48$ for Cabauw, $1.17 \pm 0.12$ for SE US, and $1.90 \pm 0.12$ for SW US. Since the activity coefficients for the US studies are similar, they were averaged to produce one curve for SE US and SW US. Averaged $\gamma_{H^+}/\gamma_{NH_4^+} = 1.6$ and $\gamma_{H^+}\gamma_{NO_3^-} = 0.087$. Some of the data scatter can be attributed to variations in liquid water, temperature, and activity coefficients. These effects are illustrated by the light gray shaded regions, which were plotted with different $W_i$, T, and $\gamma_{H^+}\gamma_{NO_3^-}$ or $\gamma_{H^+}/\gamma_{NH_4^+}$. For example, the upper line for $\varepsilon(NO_3^-)$ is calculated using $W_i = 4$ µg m$^{-3}$, T = 15 °C, and $\gamma_{H^+}\gamma_{NO_3^-} = 0.087$, while the lower line is calculated using $W_i = 1$ µg m$^{-3}$, T = 25 °C, and $\gamma_{H^+}\gamma_{NO_3^-} = 0.17$. For $\varepsilon(NH_4^+)$, the upper line for is calculated using $W_i = 4$ µg m$^{-3}$, T = 15 °C, and $\gamma_{H^+}/\gamma_{NH_4^+} = 5.93$, while the lower line is calculated using $W_i = 1$ µg m$^{-3}$, T = 25 °C, and $\gamma_{H^+}/\gamma_{NH_4^+} = 1.6$.

## 5. Temperature dependencies of NH$_3$ and HNO$_3$ gas-particle partitioning
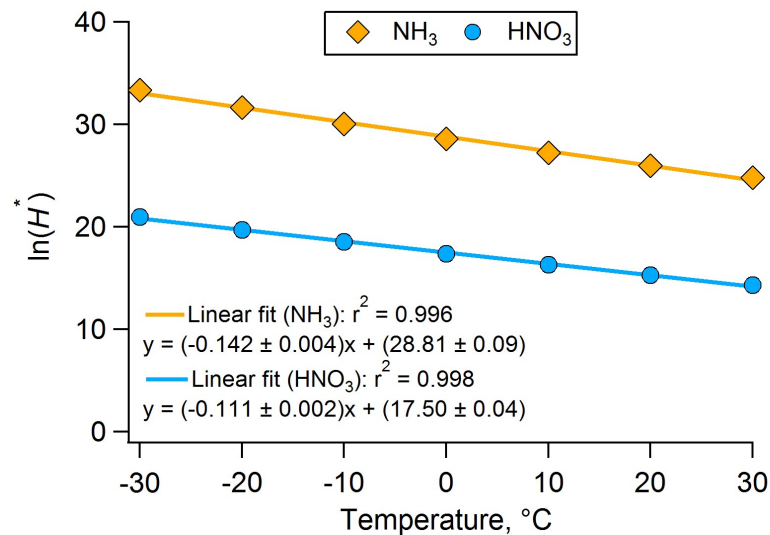
**Fig. S6.** Molality-based equilibrium constants ($H^*$) of NH$_3$-NH$_4^+$ and HNO$_3$-NO$_3^-$ partitioning as a function of temperature. $H^*_{NH_3}$ (atm$^{-1}$) is for $NH_{3(g)}+H^+ \leftrightarrow NH_4^+$ and $H^*_{HNO_3}$ (mole$^2$ kg$^{-2}$ atm$^{-1}$) is for $HNO_{3(g)} \leftrightarrow NO_3^- + H^+$. The $H^*_{NH_3}$ and $H^*_{HNO_3}$ are calculated based on Clegg et al. (1998) and Clegg and Brimblecombe (1990), respectively, with a typo correction for the equation of $H^*_{NH_3}$. The correction and some instructions to calculate $H^*$ can be found in the supplemental material of Guo et al. (2017a). $H^*_{NH_3}$ decreases faster with increasing temperature compared to $H^*_{HNO_3}$ (slope: -0.142 vs. -0.111), resulting in a net increase in particle H$^+$.

## 6. Particle nitrate and total inorganic mass reduction simulations at less sulfate or more nonvolatile cations condition
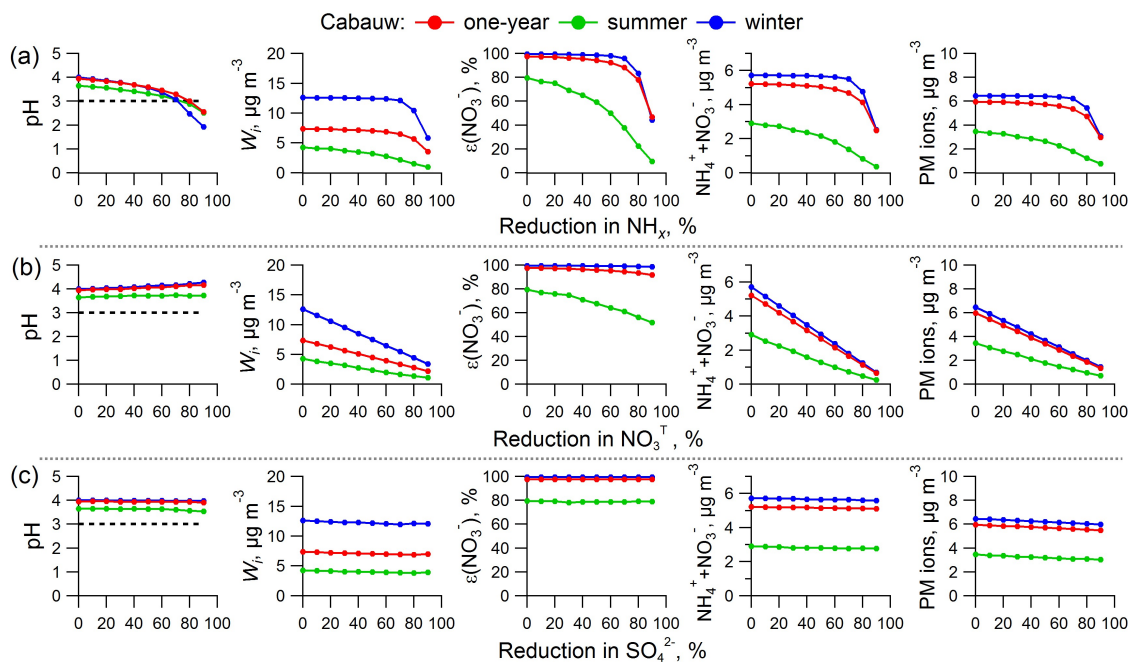
**Fig. S7.** Similar graph to Figure 4 in the main text, but for simulations with sulfate at 20% of the observed sulfate level while keeping all other inputs unchanged. The prediction of particle pH (1st column), liquid water content ($W_i$, 2nd column), nitrate particle-phase fraction ($\varepsilon(NO_3^-)$, 3rd column), ammonium and nitrate (4th column), and total aerosol inorganic mass concentrations (5th column) for reduction of $NH_x$ ($NH_4^+ + NH_3$, 1st row), $NO_3^T$ ($NO_3^- + HNO_3$, 2nd row), and $SO_4^{2-}$ (3rd row) with the base case the average conditions of one-year (July 2012-June 2013), summer (June-Aug 2012), and winter (Dec 2012-Feb 2013) observational data in Cabauw, Netherlands.
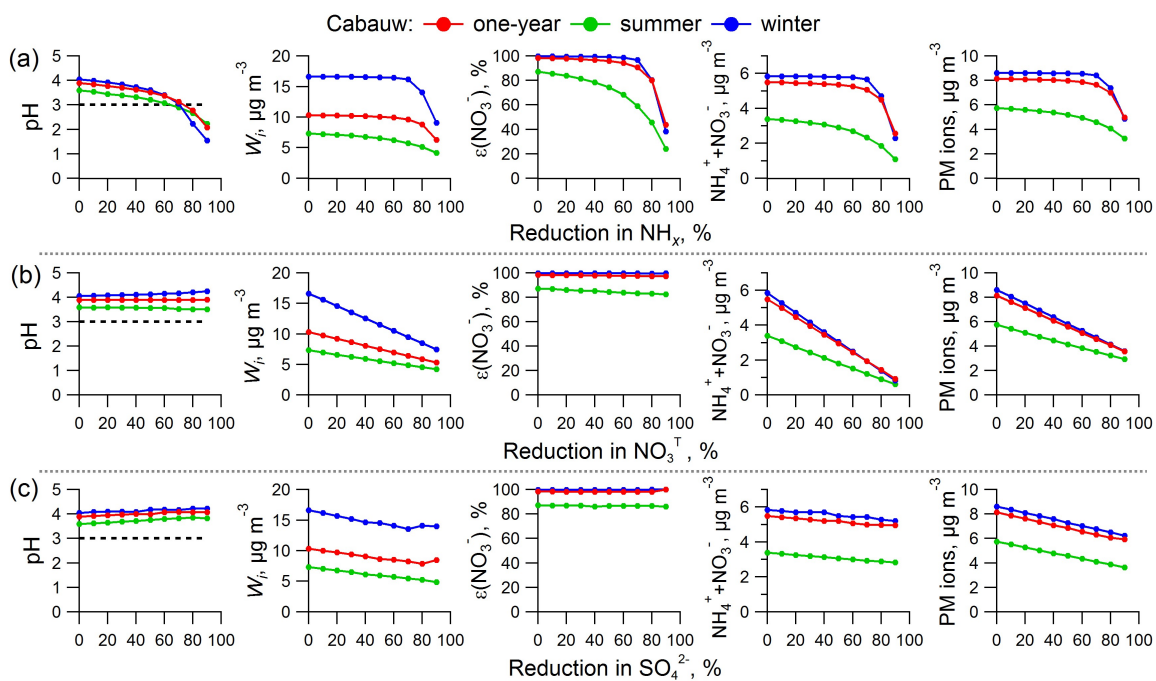
**Fig. S8.** A similar graph to Figure 4 in the main text and Fig. S4 in the supplement. The above figure shows results with five times of the observed nonvolatile cation levels, while keeping other inputs unchanged.

## 7. Summary of thermodynamic modeling inputs and outputs based on the observational averages in Cabauw, Netherlands, and previously published observational averages at several other sites.

**Table. S1.** Study average aerosol composition and meteorological conditions for various sites. Various concentrations, RH, and T are based on field measurements, unless noted specifically.

| (Region) Country | SE US | NE US | SW US | Netherlands | | | China |
|---|---|---|---|---|---|---|---|
| Site location | Centreville, AL | Hampton, VA | Pasadena, CA | Cabauw | | | Beijing |
| Campaign | SOAS | WINTER | CalNex | EU-FP7-ACTRIS (Q-ACSM Network) | | | \ |
| Sampling type | Ground | Aircraft | Ground | Ground | | | Ground |
| PM cut size | $PM_1$&$PM_{2.5}$[a] | $PM_1$ | $PM_1$[c] | $PM_{2.5}$[d] | | | $PM_1$ |
| Year | 2013 | 2015 | 2010 | 2012-2013 | | | 2013 |
| Season | Summer | Winter | (Early) Summer | One-year | Summer | Winter | Winter |
| $Na^+$, µg m$^{-3}$ | 0.03 | 0 | 0 | 0.14 | 0.17 | 0.15 | 0 |
| $SO_4^{2-}$, µg m$^{-3}$ | 1.73 | 1.02 | 2.86 | 2.20 | 1.86 | 2.51 | 26 |
| $NH_4^++NH_3$, µg m$^{-3}$ | 0.78 | 0.50 | 3.44 | 9.63 | 11.44 | 6.73 | 32.8 |
| $NO_3^-+HNO_3$, µg m$^{-3}$ | 0.45 | 2.21 | 10.22 | 4.87 | 3.48 | 5.50 | 26 |
| $Cl^-+HCl$, µg m$^{-3}$ | 0.02 | 0 | 0 | 0.53 | 0.44 | 0.54 | 1.7 |
| $Ca^{2+}$, µg m$^{-3}$ | 0 | 0 | 0 | 0.01 | 0.02 | 0.001 | 0 |
| $K^+$, µg m$^{-3}$ | 0 | 0 | 0 | 0.004 | 0.01 | 0.002 | 0 |
| $Mg^{2+}$, µg m$^{-3}$ | 0 | 0 | 0 | 0.03 | 0.01 | 0.04 | 0 |
| RH, % | 74 | 58 | 79 | 78 | 78 | 85 | 56 |
| T, °C | 24.7 | -0.4 | 18.3 | 9.0 | 17.8 | 2.4 | 0.9 |
| $NH_4^+$, µg m$^{-3}$ | 0.46 | 0.50 | 2.06 | 1.90 | 1.51 | 2.13 | 20 |
| $NH_3$, µg m$^{-3}$ | 0.39 | 0.10[b] | 1.37 | 7.73 | 9.94 | 4.60 | 12.8 |
| $\varepsilon(NH_4^+)$, % | 59 | 91[b] | 56 | 19 | 14 | 27 | 60 |
| $NO_3^-$, µg m$^{-3}$ | 0.08 | 0.80 | 3.58 | 4.53 | 3.08 | 5.28 | 26 |
| $HNO_3$, µg m$^{-3}$ | 0.36 | 1.41 | 6.65 | 0.35 | 0.40 | 0.22 | \ |
| $\varepsilon(NO_3^-)$, % | 22 | 39 | 39 | 88 | 84 | 91 | \ |
| HCl, µg m$^{-3}$ | \ | \ | \ | 0.13 | 0.16 | 0.03 | \ |
| $Cl^-$, µg m$^{-3}$ | 0.02 | 0 | 0 | 0.40 | 0.28 | 0.51 | 1.7 |
| $\varepsilon(Cl^-)$, % | \ | \ | \ | 66 | 52 | 89 | \ |
| $\gamma_{NO_3}-\gamma_{H^+}$ | 0.08 | 0.06 | 0.14 | 0.24 | 0.20 | 0.24 | 0.11[e] |
| Liquid water, µg m$^{-3}$ | 5.1 | 2.0 | 13.9 | 21.7 | 15.7 | 31.4 | 35.1[e] |
| $\Delta pH/\Delta(log_{10}NH_3)$ | 1.01 | 1.03 | 1.07 | 1.05 | 1.16 | 1.00 | 1.00[e] |
| pH | 0.9 ± 0.6 | 0.8 ± 1.0 | 1.9 ± 0.5 | 3.7 ± 0.5 | 3.3 ± 0.5 | 3.9 ± 0.4 | 4.2[e] |
| Reference | (Guo et al., 2015) | (Guo et al., 2016) | (Guo et al., 2017a) | This study | | | (Wang et al., 2016) |

Right-side braces: ISORROPIA-II input (Na⁺ through T); Input related parameters (NH₄⁺ through ε(Cl⁻)); ISORROPIA-II output ($\gamma_{NO_3}-\gamma_{H^+}$ through pH).

[a] $PM_{2.5}$ was sampled in the 1$^{st}$ half and $PM_1$ sampled in the 2$^{nd}$ half of the study; various parameters were similar in both cases, crustal components were higher in $PM_{2.5}$, but generally low so differences had minor effects, e.g., $PM_{2.5}$ $Na^+$ was 0.06 ± 0.09 µg m$^{-3}$ and $PM_1$ $Na^+$ was 0.01 ± 0.01 µg m$^{-3}$; [b] Prediction based on iteration; [c] $PM_{2.5}$ data was only available for the last week, so here we focus on $PM_1$ collected throughout the campaign; [d] $PM_1$ data is also available but not included; [e] The model results are from another publication, Guo et al. (2017b).

# References

Bougiatioti, A., Nikolaou, P., Stavroulas, I., Kouvarakis, G., Weber, R., Nenes, A., Kanakidou, M., and Mihalopoulos, N.: Particle water and pH in the Eastern Mediterranean: Sources variability and implications for nutrients availability, Atmos. Chem. Phys., 16, 4579-4591, doi: 10.5194/acp-16-4579-2016, 2016.

Clegg, S. L., and Brimblecombe, P.: Equilibrium partial pressures and mean activity and osmotic coefficients of 0-100% nitric acid as a function of temperature, Journal of Physical Chemistry, 94, 5369-5380, doi: 10.1021/j100376a038, 1990.

Clegg, S. L., Brimblecombe, P., and Wexler, A. S.: Thermodynamic model of the system $H^+$-$NH_4^+$-$SO_4^{2-}$-$NO_3^-$-$H_2O$ at tropospheric temperatures, Journal of Physical Chemistry A, 102, 2137-2154, doi: 10.1021/Jp973042r, 1998.

Fountoukis, C., and Nenes, A.: ISORROPIA II: a computationally efficient thermodynamic equilibrium model for $K^+$-$Ca^{2+}$-$Mg^{2+}$-$NH_4^+$-$Na^+$-$SO_4^{2-}$-$NO_3^-$-$Cl^-$-$H_2O$ aerosols, Atmos. Chem. Phys., 7, 4639-4659, doi: 10.5194/acp-7-4639-2007, 2007.

Guo, H., et al.: Fine-particle water and pH in the southeastern United States, Atmos. Chem. Phys., 15, 5211-5228, doi: 10.5194/acp-15-5211-2015, 2015.

Guo, H., et al.: Fine particle pH and the partitioning of nitric acid during winter in the northeastern United States, J. Geophys. Res., 121, 10355-10376, doi: 10.1002/2016jd025311, 2016.

Guo, H., Liu, J., Froyd, K. D., Roberts, J. M., Veres, P. R., Hayes, P. L., Jimenez, J. L., Nenes, A., and Weber, R. J.: Fine particle pH and gas–particle phase partitioning of inorganic species in Pasadena, California, during the 2010 CalNex campaign, Atmos. Chem. Phys., 17, 5703-5719, doi: 10.5194/acp-17-5703-2017, 2017a.

Guo, H., Weber, R. J., and Nenes, A.: High levels of ammonia do not raise fine particle pH sufficiently to yield nitrogen oxide-dominated sulfate production, Sci. Rep., 7, doi: 10.1038/s41598-017-11704-0, 2017b.

Hennigan, C. J., Izumi, J., Sullivan, A. P., Weber, R. J., and Nenes, A.: A critical evaluation of proxy methods used to estimate the acidity of atmospheric particles, Atmos. Chem. Phys., 15, 2775-2790, doi: 10.5194/acp-15-2775-2015, 2015.

Liu, M., et al.: Fine particle pH during severe haze episodes in northern China, Geophys. Res. Lett., 44, 5213-5221, doi: 10.1002/2017gl073210, 2017.

Schlag, P., Kiendler-Scharr, A., Blom, M. J., Canonaco, F., Henzing, J. S., Moerman, M., Prévôt, A. S. H., and Holzinger, R.: Aerosol source apportionment from 1-year measurements at the CESAR tower in Cabauw, the Netherlands, Atmos. Chem. Phys., 16, 8831-8847, doi: 10.5194/acp-16-8831-2016, 2016.

Wang, G., et al.: Persistent sulfate formation from London Fog to Chinese haze, Proceedings of the National Academy of Sciences of the United States of America, 113, 13630-13635, doi: 10.1073/pnas.1616540113, 2016.

Xu, L., Suresh, S., Guo, H., Weber, R. J., and Ng, N. L.: Aerosol characterization over the southeastern United States using high-resolution aerosol mass spectrometry: spatial and seasonal variation of aerosol composition and sources with a focus on organic nitrates, Atmos. Chem. Phys., 15, 7307-7336, doi: 10.5194/acp-15-7307-2015, 2015.